

RESEARCH LETTER

10.1002/2014GL062398

Key Points:

- ENSO and carbon cycle responses are analyzed under different climate conditions
- ENSO-driven anomalies are generally weaker in a warmer climate
- Changes are better detectable in carbon cycle variables than temperature

Supporting Information:

- Figures S1–S4

Correspondence to:

K. M. Keller,
keller@climate.unibe.ch

Citation:

Keller, K. M., F. Joos, F. Lehner, and C. C. Raible (2015), Detecting changes in marine responses to ENSO from 850 to 2100 C.E.: Insights from the ocean carbon cycle, *Geophys. Res. Lett.*, *42*, 518–525, doi:10.1002/2014GL062398.

Received 26 NOV 2014

Accepted 29 DEC 2014

Accepted article online 6 JAN 2015

Published online 20 JAN 2015

Detecting changes in marine responses to ENSO from 850 to 2100 C.E.: Insights from the ocean carbon cycle

Kathrin M. Keller^{1,2}, Fortunat Joos^{1,2}, Flavio Lehner^{1,2,3}, and Christoph C. Raible^{1,2}

¹Climate and Environmental Physics, Physics Institute, University of Bern, Bern, Switzerland, ²Oeschger Centre for Climate Change Research, University of Bern, Bern, Switzerland, ³Now at National Center for Atmospheric Research, Boulder, Colorado, USA

Abstract It is open whether El Niño–Southern Oscillation (ENSO) varies under climate change and how potential changes in the marine system are detectable. Here differences in the influence of ENSO on biogeochemical tracers, pH, productivity, and ocean temperature are analyzed in a continuous 850–2100 Common Era (C.E.) simulation with the Community Earth System Model. The modeled variance in ENSO amplitude is significantly higher during the Maunder Minimum cold than during the 21st century warm period. ENSO-driven anomalies in global air–sea CO₂ flux and marine productivity are two to three times lower, and ocean tracer anomalies are generally weaker in the 21st century. Significant changes are detectable in both surface and subsurface waters and are earlier verifiable and more widespread for carbon cycle tracers than for temperature. This suggests that multitracer observations of both physical and biogeochemical variables would enable an earlier detection of potential changes in marine ENSO responses than temperature-only data.

1. Introduction

El Niño–Southern Oscillation (ENSO) is the most prominent source of natural variability in the global climate system on interannual timescales, causing anomalies in winds, rainfall, circulation, thermocline depth, and biological productivity [Fiedler, 2002]. Further, it is the major driver of interannual variability in atmospheric CO₂ [Bacastow, 1976; Siegenthaler, 1990; McKinley et al., 2004].

In the last 1000 years the global climate system underwent substantial changes [e.g., Lehner et al., 2013], and the current anthropogenic warming is projected to continue [e.g., Stocker et al., 2013]. These climatic changes might have the potential to substantially affect modes of natural variability such as ENSO or the North Atlantic Oscillation [Collins et al., 2010; Li et al., 2011; Timmermann et al., 2007; Christensen et al., 2013], which has implications for biogeochemical cycles and ecosystems [Keller et al., 2012].

For ENSO, there is some evidence from reconstructions that the (late) twentieth century ENSO variance levels are not unprecedented, but higher than for any 30 year period within 1590–1880 [McGregor et al., 2013] or even the past seven centuries [Li et al., 2013]. Further, ocean reanalysis data sets record a shift of ENSO toward higher frequency since 2000 compared to 1979–1999 [Kumar and Hu, 2014]. However, while there is agreement on strong multidecadal variability in ENSO, there is no hint for a clear systematic trend over time in past ENSO variance and frequency [e.g., Emile-Geay et al., 2012; Phipps et al., 2013]. Model simulations even indicate that multidecadal variability of ENSO might arise entirely by chance [Wittenberg et al., 2014].

The detection of changes in the mean state and in climate modes is a signal-to-noise (S/N) problem [e.g., Hawkins and Sutton, 2012]. A recent study shows that for a timely detection of signals in the surface ocean, the S/N ratio of biogeochemical variables is more favorable than, e.g., sea surface temperature [Keller et al., 2014]. Further, there is a lack of studies addressing how ENSO affects air–sea fluxes of CO₂, marine productivity, ocean acidification, and biogeochemical tracers under different past, present, and future climate conditions.

Here changes in ENSO variability and related changes in the marine biogeochemical systems are diagnosed from results of the Community Earth System Model (CESM, version 1). We rely on a transient simulation over the last millennium and the 21st century driven by solar, volcanic, and anthropogenic forcings. Guiding questions are whether there are changes of ENSO characteristics under different periods and if and

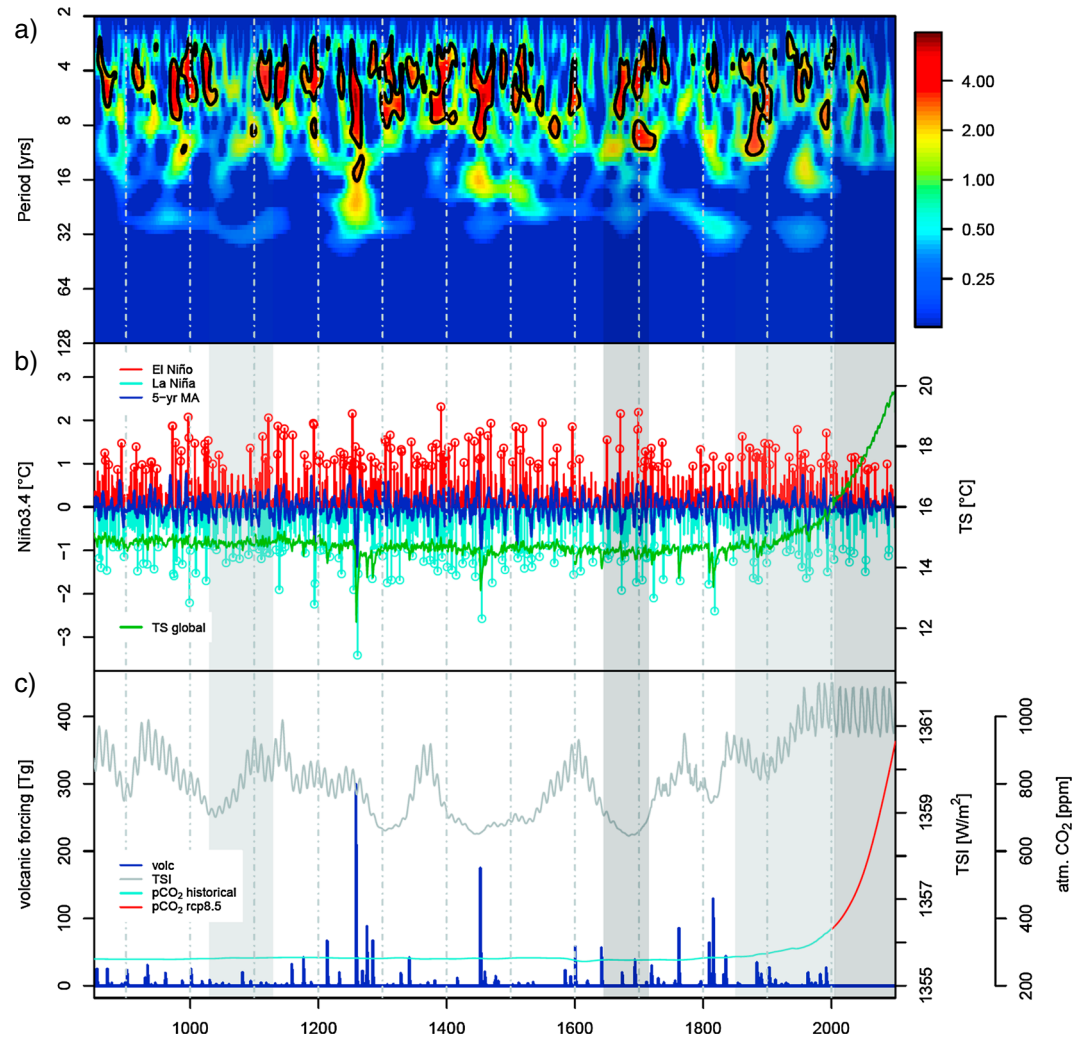


Figure 1. ENSO variability and climate forcings. (a) Wavelet spectrum based on the annual Niño3.4 SST anomalies. (b) Simulated annual and 5 year moving average of Niño3.4 index, and global surface temperature (TS). All ENSO events exceeding the threshold for the composites are marked with a circle. (c) Total solar irradiance (TSI), volcanic forcing (volc; total volcanic aerosol mass), and atmospheric CO₂ (pCO₂). The grey bars indicate the four different time periods investigated.

how such changes affect the response of physical and biogeochemical tracers, marine productivity, and air-sea carbon fluxes to ENSO in a statistically significant and detectable way.

2. Model Data and Analysis Techniques

We use a continuous 850–2100 Common Era (C.E.) simulation with CESM1.0.1 [Hurrell *et al.*, 2013]. The model is run in fully coupled mode including an interactive carbon cycle [Moore *et al.*, 2013]. The last millennium simulation was branched from a 258 year long 850 C.E. control simulation, which in turn was branched from a long 1850 C.E. control simulation with CCSM4 [Gent *et al.*, 2011]. The transient forcing largely follows the protocols of the Paleoclimate and Modelling Intercomparison Project 3 [Schmidt *et al.*, 2011], applying volcanic forcing [Gao *et al.*, 2008], land use changes [Pongratz *et al.*, 2008; Hurtt *et al.*, 2011], and fossil fuel emissions (post 1750 C.E., following Andres *et al.* [2012]). The total solar irradiance is taken from the reconstruction by Vieira and Solanki [2010] but scaled to have an amplitude change from the Maunder Minimum to present day of 0.2% rather than 0.1%. For 2005–2100 C.E., the representative concentration pathway RCP8.5 [Moss *et al.*, 2010] is used (see Figure 1c for an overview of the forcing).

ENSO here is represented by the Niño3.4 index, i.e., the spatial average of sea surface temperature (SST) anomalies in the equatorial Pacific (5°S–5°N, 170–120°W). Anomalies in all variables are obtained by

detrending the data via a spline approach (cutoff period: 40 years) [Enting, 1987]. The predecessor of CESM1, CCSM4, is known to be too sensitive to volcanic forcing [Ault *et al.*, 2013; Meehl *et al.*, 2011]. To minimize interference by this strong sensitivity, we focus on time periods without major volcanic eruptions.

We compare four different time periods: (1) 1030–1129 C.E., a period with negligible interference of strong natural or anthropogenic forcing; (2) 1645–1715 C.E., the so-called Maunder Minimum, a time period characterized by comparably low solar activity [Eddy, 1976]; (3) 1850–2005 C.E., the industrial period with strongly increasing anthropogenic forcing; and (4) 2005–2100 C.E., a period dominated by anthropogenic warming following RCP8.5. Compared to a preindustrial (850–1850) global mean surface temperature of 14.67°C, the four periods show a ΔT of +0.14°C (1030–1129), –0.16°C (1645–1715), +0.4°C (1850–2005), and +3.12°C (2005–2100).

The response of marine physical and biogeochemical variables to ENSO is quantified by a composite analysis based on monthly data. (Note that an analysis based on seasonal or annual averages provides comparable results.) The composites for El Niño and for each climatic period are computed by averaging the anomalies over time for periods where the Niño3.4 index exceeds one standard deviation (σ). The threshold σ is taken from the Maunder Minimum and applied to all periods analyzed (composites are qualitatively similar when σ is estimated for each period individually). We also calculate composites for La Niña conditions (see the supporting information for examples) but do not discuss these any further as response patterns to La Niña mirror those to El Niño in an approximately linear manner. To account for the autocorrelation of monthly data, the numbers of events (= the degrees of freedom for the statistical tests) was reduced. This results in the following numbers of events: 1030–1129 C.E., 9 El Niño/13 La Niña; Maunder Minimum, 8/12; 1850–2005 C.E., 29/29; 2005–2100 C.E., 20/22. Tests based on arbitrary 50 year periods are consistent with the results presented here. This indicates that the time periods used (70–155 years) are of sufficient length and that the results are not sensitive to the different lengths or numbers of events of the four periods.

3. Results

The model captures the observed frequency of ENSO with periodicities of 2–7 years (Figures 1a and 1b). The amplitude, however, is too strong, as was already shown for CCSM4 [Deser *et al.*, 2012]. In conjunction with major volcanic eruptions (years 1258, 1452, and 1815) we find strong La Niña events and a shift of ENSO toward lower frequencies, both also visible in the sea level pressure-based Southern Oscillation Index (not shown). These features, absent in observations and reconstructions, illustrate that CESM1 is indeed too sensitive to volcanic activity.

The amplitude of ENSO changes over time. The highest σ of annual SST anomalies in the Niño3.4 region is found for the coldest period, the Maunder Minimum (0.85°C), the lowest σ for the warmest period, 2005–2100 C.E. (0.57°C). The periods 1020–1129 C.E. (0.68°C) and 1850–2005 C.E. (0.79°C) are in between (see power spectra in the supporting information). A test of the variance reveals that Maunder Minimum and both 1030–1129 C.E. and 2005–2100 C.E. are significantly different from each other (F test, 5% level). While it is unclear whether these simulated changes are realistic, they permit us to investigate the response in different physical and biogeochemical variables to potential changes in ENSO in the self-consistent setting of an Earth System Model.

Figure 2 presents El Niño composites spanning the equatorial Pacific for anomalies of dissolved inorganic carbon (DIC), O_2 , pH, and potential ocean temperature (TEMP). All variables exhibit a seesaw pattern between east and west. We find a significant response mainly in the upper kilometer but exceptionally also down to 2000 m and below. During El Niño, the reduced upwelling in the eastern equatorial Pacific brings less carbon- and nutrient-rich waters to the surface. The resulting negative anomalies in DIC and nutrients are spreading westward along the equator. The reduction in DIC in surface waters leads to a reduction in the partial pressure of CO_2 and, consequently, in the outgassing of CO_2 to the atmosphere. This results in a positive anomaly in the net air-sea flux of CO_2 in this region (Figure 3). Similarly, the reduced input of nutrients into the euphotic zone causes a reduction in biological productivity (Figure 3) along the equator.

Statistically significant differences between the El Niño composites emerge for the different climatic periods in the equatorial Pacific (Figure 2, stippled areas). Locally significant and widespread changes are detected

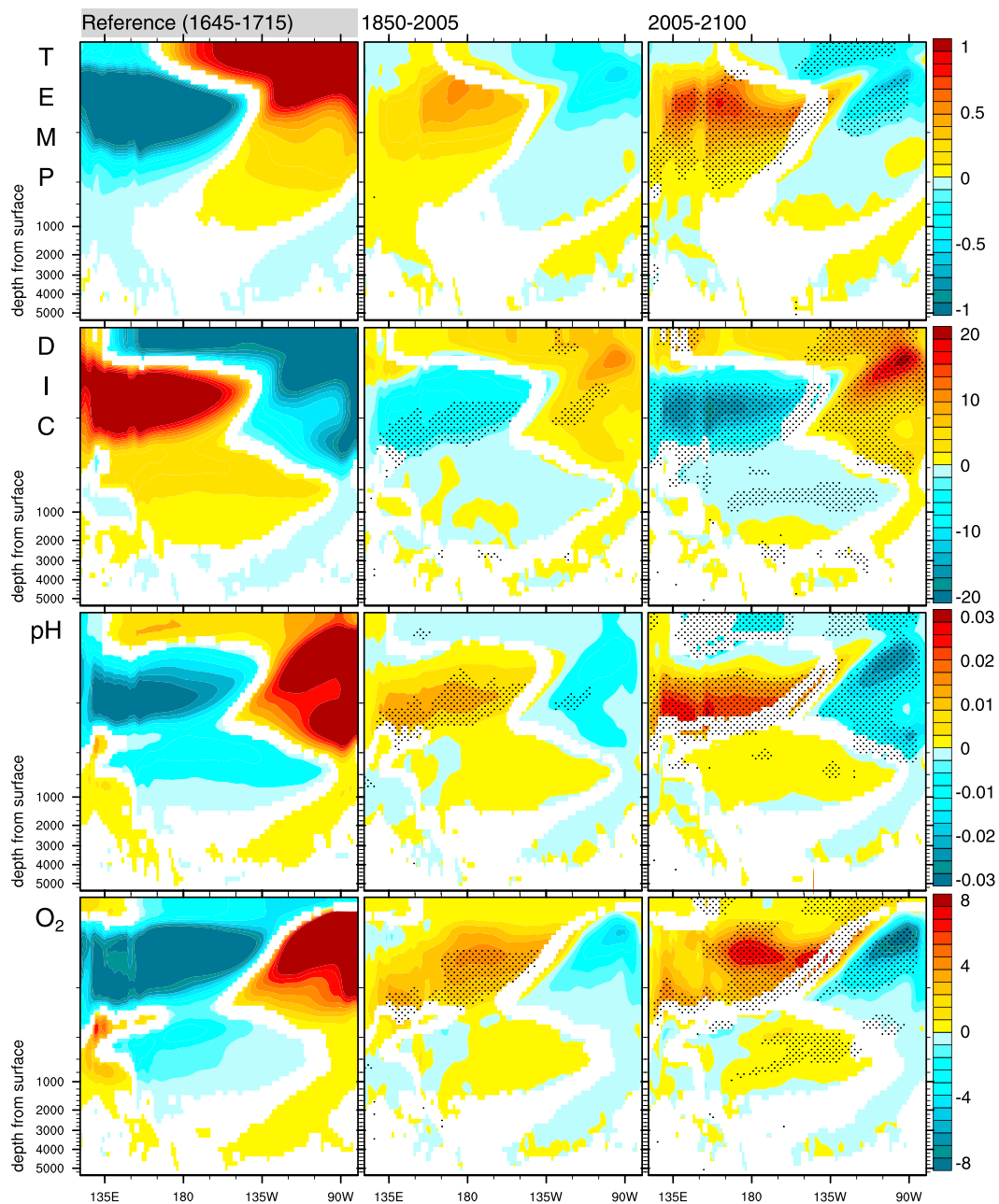


Figure 2. El Niño anomalies of potential temperature (TEMP; °C), dissolved inorganic carbon (DIC; mmol/m³), total pH, and dissolved oxygen (O₂; mmol/m³). Column 1 shows the period 1645–1715 (Maunder Minimum); columns 2 and 3 show the deviation of the periods 1850–2005 and 2005–2100 compared to this reference period (e.g., 2005–2100—Maunder Minimum). The sections span the entire equatorial Pacific and represent meridional averages (10°S–10°N). Only statistically significant values compared to the background variability are shaded (*t* test, 5% level). Stippling (1850–2005 and 2005–2100) indicates where the composites are significantly different compared to the composite 1645–1715 (*t* test, 5% level). Anomalies of 1030–1129 (not shown; see supporting information) are also weaker compared to the Maunder Minimum, however, not significantly.

in the upper kilometer between the 21st century and the Maunder Minimum period in all tracers, though significant changes are less widespread for temperature than for DIC, O₂, and pH. Locally significant changes are also detected between the industrial and the Maunder Minimum period for DIC, O₂, and pH, but not for temperature. In other words, ENSO-driven changes in biogeochemical tracers are detected earlier and in larger areas than those in temperature.

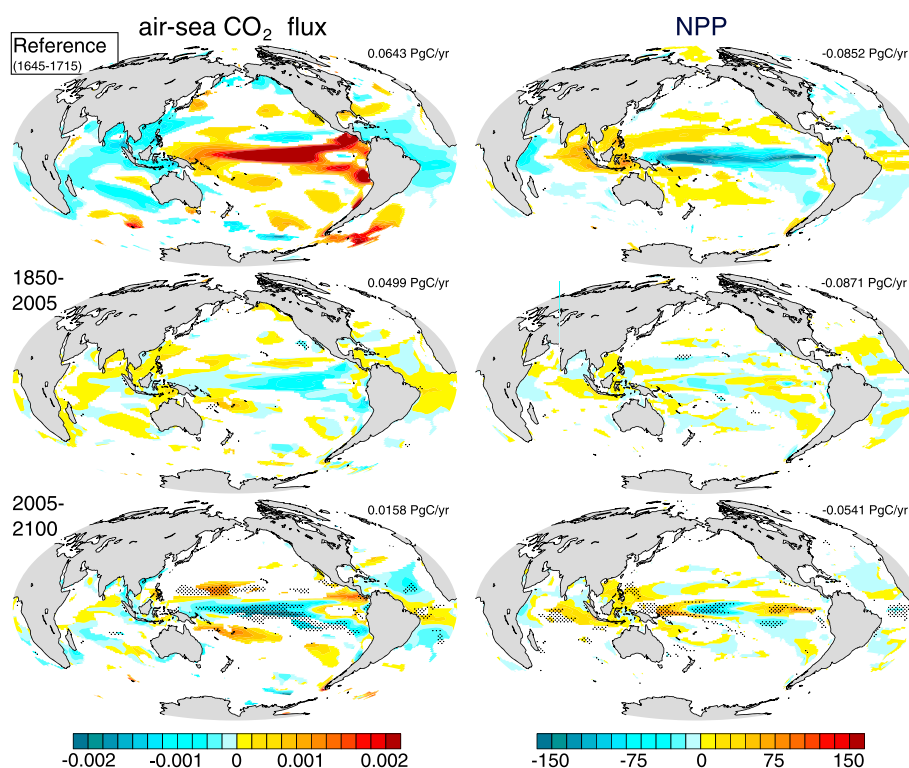


Figure 3. El Niño anomalies of air-sea CO₂ flux (mmol/m³ cm/s) and vertically (top 150 m) integrated net primary production (NPP; mgC/m²/d). Row 1 shows the period 1645–1715 (Maunder Minimum); rows 2 and 3 show the deviation of the periods 1850–2005 and 2005–2100 compared to this reference period (e.g., 2005–2100—Maunder Minimum). Only statistically significant values compared to the background variability are shaded (*t* test, 5% level). Stippling (1850–2005 and 2005–2100) indicates where the composites are significantly different compared to the composite 1645–1715 (*t* test, 5% level). The numbers represent globally integrated values (per year). Anomalies of 1030–1129 (not shown; integrated values are given in the text) are also weaker compared to the Maunder Minimum, however, not significantly.

The simulated El Niño-driven tracer anomalies are weaker during the warmer climate periods. In a warmer climate, the equatorial Pacific is subject to increasing thermal stratification and a weakening of the Walker circulation and the associated trade winds [Collins *et al.*, 2010]. Both features are present in our simulation and result in a shallower and less tilted thermocline (see supporting information for the associated decrease in mixed layer depth). Consequently, the El Niño-driven anomalies in the west do not penetrate as deep into the ocean during warm than during cold periods. The larger density gradient between surface and deeper ocean tends to hinder the penetration of the ENSO anomalies to deeper layers. In the east this behavior is less distinct. Here the Pacific-wide trend toward a shallow thermocline and the decrease in the west-east tilt of the thermocline have opposite effects on the thermocline, and changes in stratification are smaller in the East than West Pacific (Figure 4).

The weakening of the ENSO response is also visible at the surface. Figure 3 shows El Niño patterns of air-sea CO₂ flux and vertically integrated (top 150 m) net primary production (NPP). Both variables show locally significant differences in parts of the equatorial Pacific in 2005–2100 C.E., but rarely in 1850–2005 C.E., compared to 1645–1715 C.E. (Maunder Minimum). This is also the case for SST and surface DIC (see supporting information). Globally integrated NPP anomalies are much smaller in the 21st century than during the other three periods, e.g., -0.1058 pg C/yr (1030–1129 C.E.) versus -0.0541 pg C/yr (2005–2100). These values are affected by anticorrelated anomalies in the equatorial Pacific and Indian Oceans, which can be attributed to the frequent co-occurrence of ENSO and Indian Ocean Dipole (IOD) events [e.g., Currie *et al.*, 2013]. CESM1 features a correlation between ENSO and IOD of approximately 0.6, which is in agreement with the observational evidence for an occasional, however, not mandatory concurrency of the two modes [Cai *et al.*, 2014]. For the equatorial Pacific (20°S–20°N, 140°E–70°W), NPP anomalies are -0.1746 pg C/yr (1030–1129), -0.1415 pg C/yr (1645–1715), -0.1413 pg C/yr (1850–2005), and -0.1157 pg C/yr (2005–2100).

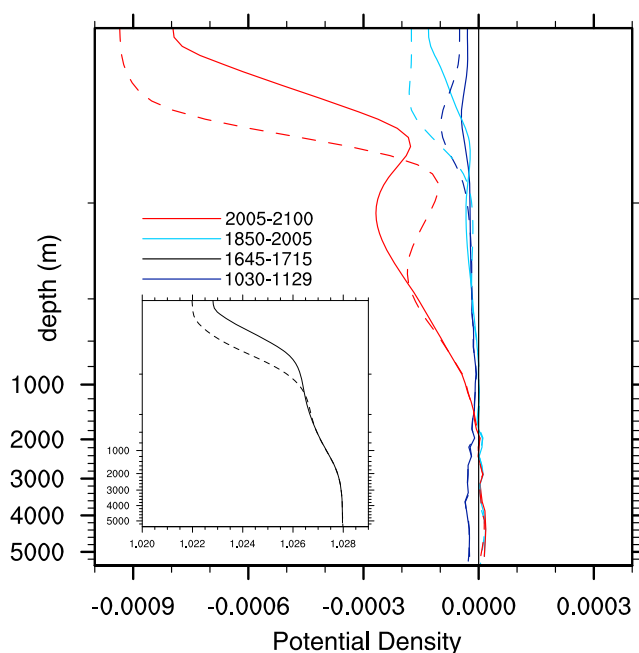


Figure 4. Profiles of potential density of all four time periods, averaged for regions in the eastern (solid; 90°–150°W, 10°S–10°N) and western (dashed; 160°E–150°W, 10°S–10°N) equatorial Pacific. The inset shows the absolute values of 1645–1715; the main plot shows the anomalies of the other three periods relative to 1645–1715.

The globally integrated net air-sea CO₂ flux reveals largest anomalies (0.0643 pg C/yr) during the coldest period, Maunder Minimum, and very small anomalies (0.0158 pg C/yr) during the warmest period, 2005–2100 C.E. The anomalies for La Niña show a comparable decrease (Maunder Minimum: -0.0638 pg C/yr; 2005–2100 C.E.: -0.0142 pg C/yr). The mean global air-sea CO₂ flux during the four periods is 0.37 pg C/yr (1030–1129), 0.38 pg C/yr (Maunder Minimum), 0.80 pg C/yr (1850–2005), and 2.62 pg C/yr (2005–2100). Hereby, the decrease in the ENSO response partly coincides with the increase of the mean air-sea CO₂ flux due to anthropogenic CO₂ emissions.

4. Discussion and Conclusions

Here we investigate changes in the ENSO-related variability of the ocean climate-carbon cycle system in a 850–2100 C.E. simulation with the Earth System Model CESM1.

The investigated periods differ in global mean surface air temperature. Yet we stress that ENSO dynamics result from the complex interplay of different background states (e.g., thermocline depth, mean zonal winds, and the east-west gradient of SST) and feedback processes (e.g., thermocline and zonal advective feedbacks) [see, e.g., Collins *et al.*, 2010; Capotondi, 2013], which confound any simple relationship between ENSO and global surface temperature. Further variability in ENSO dynamics on shorter timescales arises from westerly wind bursts [Eisenman *et al.*, 2005].

ENSO is a robust feature across all periods. The simulated amplitude of ENSO changes over time with the lowest variance in the warmest period. While it is unclear whether these simulated changes are realistic, they are in agreement with a recent modeling study (using CESM1), which identifies a connection between a decrease of the east-west gradient of SST in the equatorial Pacific, as it is projected under climate change, and a reduction of ENSO amplitude [Manucharyan and Fedorov, 2014]. The authors attributed the response of ENSO to a weakening of the Walker circulation.

In response to ENSO, significant anomalies are present in both physical and biogeochemical tracers. These anomalies constitute a seesaw pattern between east and west and range from the surface ocean down to 2000 m and below. The tracer anomaly patterns in response to El Niño and La Niña are approximately symmetric, although a recent study found nonsymmetric and nonlinear behavior in CCSM4 thermocline depth anomalies leading to an unequal duration of El Niño and La Niña events [DiNezio and Deser, 2014].

Between the different periods, we detect statistically significant differences in the ENSO response of tracers, marine productivity, and net air-sea carbon fluxes. The simulated ENSO-driven anomalies are generally weaker and do, by tendency, not penetrate as deep into the equatorial Pacific during warm compared to cold periods.

The weakening of the ENSO response is evident in globally integrated NPP and air-sea CO₂ flux, with values that diminish by a factor of between 2 and 3. The decrease in air-sea CO₂ flux anomalies toward the end of the simulation coincides with the anthropogenic increase of the mean air-sea CO₂ flux, which amplifies the impact loss of ENSO-driven variability on interannual timescales. Further, the model indicates differences in the carbon fluxes during “Eastern Pacific” (EP) and “Central Pacific” (CP) El Niño events. During the EP

type, there might be less outgassing of carbon in the equatorial Pacific than during CP El Niños, which were frequently observed in the last decade.

While ENSO itself is robust over time, significant changes in ocean physics, carbon cycle, and pH responses are found for the different periods. If applicable to reality, this has important implications for the ecosystem and might affect socioeconomic factors such as Pacific fishery [e.g., Fiedler, 2002; Chavez et al., 2011].

In the model, significant changes in response to ENSO are traceable in both surface and subsurface waters and earlier detectable and more widespread for carbon cycle variables than for physical variables such as ocean temperature. These results suggest that multitracers comprising both physical and biogeochemical variables might allow an earlier detection of changes in marine ENSO responses than physics-only approaches, which in turn might permit a more timely and cost-efficient implementation of adaptation and mitigation measures.

The additionally required measurements of carbon cycle variables could be gathered by equipping the observation systems in operation (e.g., Argo and Tropical Atmosphere-Ocean/Triangle Trans-Ocean Buoy Network) with the respective instruments. Such data would be highly valuable since observations of the ocean carbon cycle are scarce and limited in either time or space. Currently, Pacific-wide or global data sets describing the space-time variability of biogeochemical, ocean acidification, and ecosystem-relevant variables on adequate timescales are largely missing.

Acknowledgments

We thank Joachim Segsneider and an unknown reviewer for their helpful comments, Clara Deser for comments on the manuscript, and Axel Timmermann for discussion. The research leading to these results was supported through EU FP7 project CARBOCHANGE "Changes in carbon uptake and emissions by oceans in a changing climate" which received funding from the European Community's Seventh Framework Programme under grant agreement 264879. Additional support was received from the Swiss National Science Foundation through project 200020_147174. Simulations with NCAR CESM1 were carried out at the Swiss National Supercomputing Centre in Lugano, Switzerland. The model results presented in this study are available from the corresponding author upon request (keller@climate.unibe.ch).

The Editor thanks two anonymous reviewers for their assistance in evaluating this paper.

References

- Andres, R. J., et al. (2012), A synthesis of carbon dioxide emissions from fossil-fuel combustion, *Biogeosciences*, *9*, 1845–1871.
- Ault, T. R., C. Deser, M. Newman, and J. Emile-Geay (2013), Characterizing decadal to centennial variability in the equatorial Pacific during the last millennium, *Geophys. Res. Lett.*, *40*, 3450–3456, doi:10.1002/grl.50647.
- Bacastow, R. B. (1976), Modulation of atmospheric carbon dioxide by the Southern Oscillation, *Nature*, *261*, 116–118.
- Cai, W., A. Santoso, G. Wang, E. Weller, L. Wu, K. Ashok, Y. Masumoto, and T. Yamagata (2014), Increased frequency of extreme Indian Ocean Dipole events due to greenhouse warming, *Nature*, *510*, 254–258.
- Capotondi, A. (2013), ENSO diversity in the NCAR CCSM4 climate model, *J. Geophys. Res. Oceans*, *118*, 4755–4770, doi:10.1002/jgrc.20335.
- Chavez, F. P., M. Messie, and J. T. Pennington (2011), Marine primary production in relation to climate variability and change, *Annu. Rev. Mar. Sci.*, *3*, 227–260.
- Christensen, J., et al. (2013), Climate phenomena and their relevance for future regional climate change, in *Climate Change 2013: The Physical Science Basis. Contribution of Working Group I to the Fifth Assessment Report of the Intergovernmental Panel on Climate Change*, edited by T. F. Stocker et al., Cambridge Univ. Press, Cambridge, U. K., and New York.
- Collins, M., et al. (2010), The impact of global warming on the tropical Pacific Ocean and El Niño, *Nat. Geosci.*, *3*, 391–397.
- Currie, J. C., M. Lengaigne, J. Vialard, D. M. Kaplan, O. Aumont, S. W. A. Naqvi, and O. Maury (2013), Indian Ocean Dipole and El Niño/Southern Oscillation impacts on regional chlorophyll anomalies in the Indian Ocean, *Biogeosciences*, *10*, 6677–6698.
- Deser, C., A. S. Phillips, R. A. Tomas, Y. M. Okumura, M. A. Alexander, A. Capotondi, J. D. Scott, Y.-O. Kwon, and M. Ohba (2012), ENSO and Pacific decadal variability in the Community Climate System Model Version 4, *J. Clim.*, *25*, 2622–2651.
- DiNezio, P. N., and C. Deser (2014), Nonlinear controls on the persistence of La Niña, *J. Clim.*, *27*(19), 7335–7355.
- Eddy, J. A. (1976), Maunder minimum, *Science*, *192*, 1189–1202.
- Eisenman, I., L. Yu, and E. Tziperman (2005), Westerly wind bursts: ENSO's tail rather than the dog?, *J. Clim.*, *18*, 5224–5238.
- Emile-Geay, J., K. M. Cobb, M. E. Mann, and A. T. Wittenberg (2012), Estimating central equatorial Pacific SST variability over the past millennium. Part II: Reconstructions and implications, *J. Clim.*, *26*, 2329–2352.
- Enting, I. G. (1987), On the use of smoothing splines to filter CO₂ data, *J. Geophys. Res.*, *92*, 10,977–10,984.
- Fiedler, P. (2002), Environmental change in the eastern tropical Pacific Ocean: Review of ENSO and decadal variability, *Mar. Ecol.*, *244*, 265–283.
- Gao, C., A. Robock, and C. Ammann (2008), Volcanic forcing of climate over the past 1500 years: An improved ice core-based index for climate models, *J. Geophys. Res.*, *113*, D23111, doi:10.1029/2008JD010239.
- Gent, P. R., et al. (2011), The Community Climate System Model version 4, *J. Clim.*, *24*, 4973–4991.
- Hawkins, E., and R. Sutton (2012), Time of emergence of climate signals, *Geophys. Res. Lett.*, *39*, L01702, doi:10.1029/2011GL050087.
- Hurrell, J. W., et al. (2013), The Community Earth System Model: A framework for collaborative research, *Bull. Am. Meteorol. Soc.*, *94*, 1339–1360.
- Hurt, G., et al. (2011), Harmonization of land-use scenarios for the period 1500–2100: 600 years of global gridded annual land-use transitions, wood harvest, and resulting secondary lands, *Clim. Change*, *109*, 117–161.
- Keller, K. M., et al. (2012), Variability of the ocean carbon cycle in response to the North Atlantic Oscillation, *Tellus Ser. B*, *64*, 18,738, doi:10.3402/tellusb.v64i0.18738.
- Keller, K. M., F. Joos, and C. C. Raible (2014), Time of emergence of trends in ocean biogeochemistry, *Biogeosciences*, *11*, 3647–3659.
- Kumar, A., and Z.-Z. Hu (2014), Interannual and interdecadal variability of ocean temperature along the equatorial Pacific in conjunction with ENSO, *Clim. Dyn.*, *42*, 1243–1258.
- Lehner, F., A. Born, C. C. Raible, and T. F. Stocker (2013), Amplified inception of European Little Ice Age by sea ice-ocean-atmosphere feedbacks, *J. Clim.*, *26*, 7586–7602.
- Li, J., S.-P. Xie, E. R. Cook, G. Huang, R. D'Arrigo, F. Liu, J. Ma, and X.-T. Zheng (2011), Interdecadal modulation of El Niño amplitude during the past millennium, *Nat. Clim. Change*, *1*, 114–118.
- Li, J., S.-P. Xie, E. R. Cook, M. S. Morales, D. A. Christie, N. C. Johnson, F. Chen, R. D'Arrigo, A. M. Fowler, X. Gou, and K. Fang (2013), El Niño modulations over the past seven centuries, *Nat. Clim. Change*, *3*, 822–826.
- Manucharyan, G. E., and A. V. Fedorov (2014), Robust ENSO across a wide range of climates, *J. Clim.*, *27*, 5836–5850.

- McGregor, S., A. Timmermann, M. H. England, O. Elison Timm, and A. T. Wittenberg (2013), Inferred changes in El Niño-Southern Oscillation variance over the past six centuries, *Clim. Past*, *9*, 2269–2284.
- McKinley, G., C. Rodenbeck, M. Gloor, S. Houweling, and M. Heimann (2004), Pacific dominance to global air-sea CO₂ flux variability: A novel atmospheric inversion agrees with ocean models, *Geophys. Res. Lett.*, *31*, L22308, doi:10.1029/2004GL021069.
- Meehl, G. A., et al. (2011), Climate system response to external forcings and climate change projections in CCSM4, *J. Clim.*, *25*, 3661–3683.
- Moore, J. K., K. Lindsay, S. C. Doney, M. C. Long, and K. Misumi (2013), Marine ecosystem dynamics and biogeochemical cycling in the Community Earth System Model [CESM1(BGC)]: Comparison of the 1990s with the 2090s under the RCP4.5 and RCP8.5 scenarios, *J. Clim.*, *26*, 9291–9312.
- Moss, R. H., et al. (2010), The next generation of scenarios for climate change research and assessment, *Nature*, *463*, 747–756.
- Phipps, S. J., H. V. McGregor, J. Gergis, A. J. E. Gallant, R. Neukom, S. Stevenson, D. Ackerley, J. R. Brown, M. J. Fischer, and T. D. van Ommen (2013), Paleoclimate data-model comparison and the role of climate forcings over the past 1500 years, *J. Clim.*, *26*, 6915–6936.
- Pongratz, J., C. Reick, T. Raddatz, and M. Claussen (2008), A reconstruction of global agricultural areas and land cover for the last millennium, *Global Biogeochem. Cycles*, *22*, GB3018, doi:10.1029/2007GB003153.
- Schmidt, G. A., et al. (2011), Climate forcing reconstructions for use in PMIP simulations of the last millennium (v1.0), *Geosci. Model Dev.*, *4*, 33–45.
- Siegenthaler, U. (1990), Biogeochemical cycles—El Niño and atmospheric CO₂, *Nature*, *345*, 295–296.
- Stocker, T., et al. (2013), Technical summary, in *Climate Change 2013: The Physical Science Basis. Contribution of Working Group I to the Fifth Assessment Report of the Intergovernmental Panel on Climate Change*, edited by T. F. Stocker et al., Cambridge Univ. Press, Cambridge, U. K., and New York.
- Timmermann, A., S. J. Lorenz, S.-I. An, A. Clement, and S.-P. Xie (2007), The effect of orbital forcing on the mean climate and variability of the Tropical Pacific, *J. Clim.*, *20*, 4147–4159.
- Vieira, L. E. A., and S. K. Solanki (2010), Evolution of the solar magnetic flux on time scales of years to millenia, *Astron. Astrophys.*, *509*, A100, doi:10.1051/0004-6361/200913276.
- Wittenberg, A. T., A. Rosati, T. L. Delworth, G. A. Vecchi, and F. Zeng (2014), ENSO modulation: Is it decadal predictable?, *J. Clim.*, *27*, 2667–2681.